HHS Public Access

Author manuscript

Nat Neurosci. Author manuscript; available in PMC 2019 February 13.

Published in final edited form as:

Nat Neurosci. 2018 September ; 21(9): 1229–1238. doi:10.1038/s41593-018-0204-3.

Voluntary urination control by brainstem neurons that relax the urethral sphincter

Jason Keller[1,2], **Jingyi Chen**[1,3], **Sierra Simpson**[1,3], **Eric Hou-Jen Wang**[4], **Varoth Lilascharoen**[4], **Olivier George**[1], **Byung Kook Lim**[5], and **Lisa Stowers**[1,*]

[1]Department of Molecular and Cellular Neuroscience, The Scripps Research Institute, La Jolla, California, USA

[2]Neurosciences Graduate Program, University of California San Diego, La Jolla, California, USA

[3]Biomedical Sciences Graduate Program, The Scripps Research Institute, La Jolla, California, USA

[4]Biomedical Sciences Graduate Program, University of California San Diego, La Jolla, California, USA

[5]Neurobiology Section, Division of Biological Sciences, University of California San Diego, La Jolla, California, USA

Abstract

Voluntary urination ensures that waste is eliminated when safe and socially appropriate, even without a pressing urge. Uncontrolled urination, or incontinence, is a common problem with few treatment options. Normal urine release requires a small region in the brainstem known as Barrington's nucleus (Bar), but specific neurons that relax the urethral sphincter and enable urine flow are unknown. Here we identify a small subset of novel Bar neurons that control the urethral sphincter in mice. These excitatory neurons express estrogen receptor 1 (Bar^{ESR1}), project to sphincter-relaxing interneurons in the spinal cord and are active during natural urination. Optogenetic stimulation of Bar^{ESR1} neurons rapidly initiates sphincter bursting and efficient voiding in anesthetized and behaving animals. Conversely, optogenetic and chemogenetic inhibition reveals their necessity in motivated urination behavior. The identification of these cells provides an expanded model for the control of urination and its dysfunction.

*Corresponding Author: stowers@scripps.edu.

Competing financial interests statement

The authors declare no competing interests.

Author contributions

J.A.K., J.C., and L.S. designed the study, analyzed the data, and wrote the manuscript. S.S. aided in the cystometry (O.G. supported S.S.). E.H.W and B.K.L. aided in the fiber photometry. V.L. performed slice physiology. All other experiments were performed by J.A.K. and J.C.

Introduction

Urination (aka. micturition) is a fundamental behavior that requires coordination of the bladder and urethral sphincter[1–3]. Humans urinate involuntarily and reflexively at birth but acquire voluntary control with learning and development. Unfortunately, this motivated control is ultimately disrupted in one in three adults worldwide[4]. The neurons in the brain that control urination remain obscure, partly because most studies have focused on reflex urination, where bladder filling and voiding can be easily controlled and monitored in anesthetized animals. However, voluntary urination occurs *before* the bladder reaches capacity and must be studied in awake, behaving animals. Because of this experimental complication, there is little understanding of the neural substrates underlying natural, voluntary urination behavior and continence.

House pets commonly demonstrate that many animals, in addition to humans, can learn to control urination behavior. Moreover, territorial males of many wild animals including fish[5], rodents[6,7], and primates[8] deliberately urinate their domain to transmit social scents such as pheromones. Male mice in particular scent-mark prolifically[7,6] in order to attract female mating partners. However, exuberant urination behavior is metabolically wasteful[9] and may attract other aggressive males[10] or predators[11]. Mice offset these risks by limiting voluntary scent marks to critical social environments such as those most likely to contain females[6]. Therefore, the use of female odor to promote rapid and robust scent marking behavior in the male mouse serves as an experimental platform to identify neurons controlling voluntary urination.

The switch from urine storage to deliberate elimination is known to depend on brain input, as spinal cord injury acutely prevents voluntary urination. Barrington's nucleus (Bar, aka. pontine micturition center, PMC, M-region), is a well-conserved and heterogeneous population of neurons in the dorsal pons that was identified as the major brain center regulating urination almost a century ago[12,13]. Bar contains at least three different cell types defined by physiology[14], gene expression[13,15], and histology[13,16,17]. The best-studied among these express corticotropin releasing hormone/factor (CRH or CRF)[18–20,2]. Bar^{CRH} neurons increase their firing rate under anesthetized bladder and colon distension as well as during awake, diuretic-induced urination[21,15]. Moreover, optogenetic stimulation of these neurons generates an increase in bladder pressure[15]. However, the smooth muscle of the bladder wall contracts slowly via autonomic, involuntary control, which alone is not sufficient for voiding. Urine release is ultimately gated by the external urethral sphincter (EUS), which is normally constricted but relaxes to allow urine flow (Fig. 1a). In humans, this relaxation precedes bladder contraction and initiates voluntary urination[22,23]. The EUS is composed of striated muscle to permit fast control via somatic, voluntary motoneurons, which are monosynaptically inhibited by interneurons in the dorsal grey commissure (DGC) in the spinal cord[24–26]. Broad electrical or chemical stimulation of Bar drives urination[27,28], and current models assume that this occurs through a single, divergent Bar projection to the spinal cord to control both bladder and EUS[1,15]. However, Bar neurons that relax the urethral sphincter have not been identified.

Here we establish a voluntary urination assay in male mice by quantifying their rapid generation of scent marks following detection of female odor. We find that this behavior depends upon a previously uncharacterized subpopulation of spatially clustered neurons in Bar that express high levels of estrogen receptor 1 (Bar^{ESR1}). These neurons project heavily to the DGC and increase their activity in freely behaving mice just prior to voluntary scent marking urination. Bar^{ESR1} neurons drive efficient voiding when photostimulated in awake animals, and urinary muscle recordings in anesthetized animals indicate a unique mechanistic role in urethral sphincter relaxation. Chemogenetic inhibition of Bar^{ESR1} but not Bar^{CRH} neurons abolishes natural scent-marking urination, and acute Bar^{ESR1} photoinhibition abruptly terminates ongoing EUS relaxation. Thus, Bar^{ESR1} neurons are indispensable for driving urethral relaxation and voluntary urination in male mice and provide a promising tool for the future study of continence and incontinence.

Results

A novel cell type in Barrington's nucleus with a role in urination

Our initial tests and a previous study of Bar^{CRH} neural function showed modest effects on urination in awake animals[15], suggesting that they are unlikely to facilitate voluntary urination. Approximately half of the Bar neurons projecting to the spinal cord lack CRH expression[19], and their molecular identity and function is undetermined[13]. We took a candidate approach to identify molecular markers for Bar neurons that may function to promote urinary sphincter relaxation, and focused on estrogen receptor 1 (ESR1, ERα), as it is expressed in a subset of Bar cells in both mice[17] and primates[29]. It is unknown if ESR1 marks a cell type distinct from Bar^{CRH}. Immunostaining for ESR1 protein in CRH-Cre x ROSA-LSL-tdTomato (CRH-tdT) individuals confirmed a small Bar subpopulation (~200 cells) expressing high amounts of ESR1 (Bar^{ESR1} neurons, Fig. 1b–f). The majority of Bar^{ESR1} neurons (~3/4 of the Bar^{ESR1} population, Fig. 1f) do not overlap with CRH-tdT, and the overlapping minority likely represents an upper bound on co-expression since tdT integrates *Crh* promoter activity over the lifetime of the animal. Bar^{ESR1} neurons are found in a dorsal cluster within the Nissl-defined ovoid Bar nucleus, whereas Bar^{CRH} neurons are more numerous (~500 cells[15]), ventrally biased, and extend further along the rostrocaudal axis beyond traditional, Nissl-defined Bar borders (Fig. 1d–e). Moreover, in ESR1-Cre mice, 96.8 % of Bar^{ESR1} neurons (n=3 mice) overlap with reporter expression (Supplementary Fig. 1a), confirming that the *Crh* and *Esr1* promoters are active in largely independent Bar populations.

To investigate the potential for Bar^{ESR1} neurons to relax the urethral sphincter, we evaluated their neurotransmitter identity and anatomical connections to the lower urinary tract. Immunostaining for αESR1 in Vgat-Cre and Vglut2-Cre mouse lines crossed to fluorescent reporters, as well as in-situ hybridization, revealed that the majority of Bar^{ESR1} neurons express Vglut2 (93.6 % reporter overlap, n=3 mice) and not Vgat (2.2 % reporter overlap, n=4 mice; Supplementary Fig. 1b–k). Injection of the retrograde tracer CTB into the lumbosacral spinal cord resulted in co-expression with Bar^{ESR1} cells, indicating their direct projections to urinary targets (Supplementary Fig. 1l–n). To further investigate Bar^{ESR1} axonal projections, we unilaterally injected AAV expressing Cre-dependent GFP into the

Bar of ESR1-Cre or CRH-Cre animals, and imaged the lower thoracic to sacral spinal cord (Fig. 1g, h, j). The lumbosacral mediolateral column (ML) contains preganglionic autonomic neurons that excite the bladder (along with intermingled interneurons)[1,26], and the lumbosacral dorsal grey commissure (DGC) contains interneurons that directly inhibit (relax) sphincter motorneurons of the dorsolateral nucleus via Bar input[24–26] (Fig. 1k). Consistent with the known role in bladder pressure regulation, $Bar^{CRH\text{-}GFP}$ axons showed a dense focal projection to the ML (Fig. 1g–h top row, l) with only sparse fibers arching further medially or to thoracolumbar levels T13-L2 (Supplementary Fig. 2a–b). $Bar^{ESR1\text{-}GFP}$ axons projected similarly across the lumbosacral ML, with additional lighter fibers seen in the thoracolumbar ML (Supplementary Fig. 2c). However, they also provided much denser innervation of the sphincter-inhibiting DGC, extending rostrally from the proposed L3-L4 burst generator[30] to mid-sacral levels (Fig. 1g–h bottom row, l; Supplementary Fig. 2c). Bilateral labeling of Bar^{ESR1} or Bar^{CRH} neurons with a second Cre-dependent virus (AAV-FLEX-ChR2) confirmed the same projection patterns (Fig. 1i; Supplementary Fig. 2b–c). Thus, the cell body distribution, molecular expression, and efferents of Bar^{ESR1} neurons indicate that they constitute an uncharacterized cell type within Bar[13], distinct from Bar^{CRH} neurons.

Upon detecting the odor of a female, male mice promptly urinate to show their command of the territory and advertise their availability to mate[7,31]. We promote this voluntary urination by adding female odor (female urine) to an arena lined with absorbent paper and record the male's position from above and their urine output from below. This enables quantification of both the timing and abundance of voluntary urination events during freely moving behavior (Supplementary Fig. 3). To determine the temporal activation of Bar^{ESR1} cells in relationship to this natural urination behavior, we unilaterally injected Bar with AAV-FLEX-GCaMP6s in ESR1-Cre animals and imaged population calcium activity with fiber photometry (Fig. 2a–b). We observed robust, discrete increases in fluorescence that were highly correlated with detected urination events, compared to randomly chosen intervals (Fig. 2c–e). The lags for maximal cross correlation between urine detection and GCaMP fluorescence transients revealed no significant difference between the timing of Bar^{ESR1} population activity and urine marks (GCaMP precedes by 0.37 ± 0.16 seconds, mean ± s.e.m., n=76 urination events across 7 mice, $p = 0.18$, Wilcoxon signed rank test). Altogether, we find that ESR1 defines a novel cell type in Bar with anatomical and physiological features consistent with a direct role in urination.

Artificial activation of Bar^{ESR1} neurons promotes urination in awake and anesthetized animals

$Bar^{CRH\text{-}ChR2}$ photostimulation was previously shown to drive bladder pressure increases during urethane-anesthetized cystometry[15], but the sufficiency of these cells in awake urination has not been characterized. To determine if either of these distinct Bar populations promote urination in behaving animals, we first bilaterally infected Bar^{ESR1} or Bar^{CRH} neurons with AAV-FLEX-ChR2 or -GFP ($Bar^{ESR1\text{-}ChR2}$, $Bar^{ESR1\text{-}GFP}$, or $Bar^{CRH\text{-}ChR2}$, Fig. 3a–c) and performed slice recordings to confirm that both $Bar^{ESR1\text{-}ChR2}$ and $Bar^{CRH\text{-}ChR2}$ neurons reliably responded to photostimulation at frequencies previously used in electrical stimulation (Supplementary Fig. 4). We then quantified and compared the latency and

amount of urine induced by photostimulation in awake, freely-moving individuals *without* urine-promoting odor cues. While photostimulation of GFP-infected individuals produced no effect on urine excretion, $Bar^{ESR1\text{-}ChR2}$ stimulation led to robust, frequency-dependent urine volume released, following light onset with a mean latency of 2.1 seconds (Fig. 3d–h; Suppl. Video 1). Over 96% of $Bar^{ESR1\text{-}ChR2}$ stimulation trials at 10–50 Hz resulted in urination (Fig. 3d, f). In comparison, photostimulation of $Bar^{CRH\text{-}ChR2}$ neurons during freely-moving behavior had a much smaller effect on urination despite generally higher ChR2 viral infection levels (Fig. 3c–h; Suppl. Video 2). Less than 37% of $Bar^{CRH\text{-}ChR2}$ stimulation trials at 10–50 Hz resulted in the voiding of urine (Fig. 3f). Of this subset, the latency and amount of urine produced differed from $Bar^{ESR1\text{-}ChR2}$ at all frequencies tested (Fig. 3d–h). We additionally investigated the extent to which Bar^{ESR1} and Bar^{CRH} neural activity could initiate voiding without conscious sensory input. Photostimulation under isoflurane anesthesia, known to depress reflex urination[32,33], resulted in urine voiding in 43% of the $Bar^{ESR1\text{-}ChR2}$ trials, but only 6% of the $Bar^{CRH\text{-}ChR2}$ trials, with none of the $Bar^{CRH\text{-}ChR2}$ voids occurring during the photostimulus window (Fig. 3f, i; Suppl. Video 3). This indicates that Bar^{ESR1} neuronal activity induces rapid and efficient urination and hints at a distinct mechanism from neighboring Bar^{CRH} activity that is known to increase bladder pressure.

Bar^{ESR1} neurons drive urination by controlling the urethral sphincter

To directly test the effect of Bar^{ESR1} and Bar^{CRH} neurons on urinary muscle targets, we performed external urethral sphincter (EUS) electromyography (EMG) and cystometry (bladder filling and pressure recording) under isoflurane anesthesia (Fig. 4a). We perfused saline at a constant rate into the bladder to stimulate reflex voiding and observed natural cycles of bladder pressure increase and associated EUS bursting muscle patterns, which correlated with voiding and subsequent bladder pressure decrease (Fig. 4b). In rodents, these bursting contractions interspersed with periods of muscle relaxation are believed to enable efficient urine flow through the narrow rodent urethra[34,35]. Following observation of regular cystometry cycles, we stopped the saline pump when the bladder was “filled” or “empty” (75% or 10% of the volume observed to trigger reflex urination, respectively) and initiated 5 seconds of photostimulation (Fig. 4b, blue arrows). We found that both $Bar^{ESR1\text{-}ChR2}$ and $Bar^{CRH\text{-}ChR2}$ photostimulation produced reliable, time-locked bladder pressure increases at similar latencies (Fig. 4c–d). The initial latency and slope of the bladder pressure increase by stimulation of each cell type was indistinguishable by our analysis; however, the peak pressure and end pressure (25 seconds after stimulus onset) were significantly less for $Bar^{ESR1\text{-}ChR2}$ photostimulation. This difference occurs because only with the $Bar^{ESR1\text{-}ChR2}$ photostimulation did we observe abundant urine release, which results in a sharp pressure decrease below the starting value (Fig. 4c–f; Suppl. Video 4). When $Bar^{CRH\text{-}ChR2}$ photostimulation ceased, the bladder usually returned to the same pressure level observed prior to $Bar^{CRH\text{-}ChR2}$ stimulation (Fig 3c–d, f), independently confirming our observations that significant urine release does not normally occur through activation of this cell population (Suppl. Video 5).

The reason for the observed differences in photostimulated urine release only become clear when examining the EUS EMG responses. The photostimulated urination in $Bar^{ESR1\text{-}ChR2}$

mice coincided with a reliable bursting pattern of sphincter activity, the extent of which was dependent on bladder fill level (Fig. 5a–b; Supplementary Fig. 5a–b). Pulsatile urination occurred during the bursting periods (Suppl. Video 4), consistent with previous observations of urine flow during the relaxation periods between bursts[34,35] and our calculations of relaxation time between burstlets (Fig. 5c–d). Frequency analysis of the sphincter EMG signal also shows that 85% of the $Bar^{ESR1\text{-}ChR2}$ stimulations with a filled bladder resulted in sphincter relaxation/bursting and associated voiding (Fig. 5e–f; Supplementary Fig. 5a–b). Additionally, we observed burst-like EMG responses in the absence of bladder contractions on a subset of empty bladder trials (Supplementary Fig. 6), such that the effect of Bar^{ESR1} neurons on the sphincter cannot be solely due to reflex activity from bladder afferents. In contrast, photostimulation of $Bar^{CRH\text{-}ChR2}$ neurons produced either no detectible change in sphincter activity, tonic sphincter discharge (constriction), or rare irregular bursting (13% of trials), which was always preceded by tonic (constricting) activity and accompanied by bladder pressure increase (Fig. 5b, c–e). This tonic activity increase was characteristic of a spinal guarding reflex, a compensatory tonic contraction of the EUS mediated through bladder afferents to prevent urination during bladder distension.

The extent to which urethral sphincter bursting occurs during natural, awake rodent behavior varies across sex and species[34–37] and remains controversial. Thus, to investigate natural sphincter activity, we surgically implanted a wireless pressure recorder into the corpus spongiosum that surrounds the urethra and can serve as a proxy for the urethral activity, where bursting duration corresponds to the amount of urine release[38]. Upon recovery, we analyzed the urination behavior in response to odor cues and found urethral sphincter bursting patterns to occur during the awake behavior (Supplementary Fig. 5c–f). Notably, the duration and slope of the spectral power seen during the $Bar^{ESR1\text{-}ChR2}$ photostimulation bursts mimicked wirelessly recorded pressure during awake, natural scent-marking urination (Supplementary Fig. 5b, e, f). Overall, these awake and anesthetized urinary recordings indicate that stimulation of both Bar populations equally increase bladder pressure, but only Bar^{ESR1} neurons relax the EUS via bursting to enable efficient urine flow as in natural, awake urination in male mice.

Bar^{ESR1} but not Bar^{CRH} neurons are indispensable for voluntary scent marking urination

No single cell type in Bar has been shown to be necessary for voluntary urination. To investigate the extent to which Bar neurons participate in this motivated behavior, we established a rapid behavioral assay that compares the voluntary baseline urination rate (two minutes in the presence of a control odor) to the rate during the subsequent two minutes, in the presence of motivating female urine odor (Fig. 6; Suppl. Video 6). The reliable and rapid change in the amount of urine marks in response to female urine indicates that olfactory cues access circuits which relax the EUS and generate voluntary urination.

To test if Bar neurons are necessary for this response, we bilaterally infected them with AAV-FLEX-hM4Di in ESR1-Cre or CRH-Cre mice ($Bar^{ESR1\text{-}hM4Di}$ or $Bar^{CRH\text{-}hM4Di}$; Fig. 7a–b). Individuals were then injected with either CNO or saline on alternate days and assayed for their urination rate in the presence of female urine. Female-odor evoked urination was reversibly diminished following CNO injections in $Bar^{ESR1\text{-}hM4Di}$ but not

$Bar^{CRH\text{-}hM4Di}$ or wild-type control mice (Fig. 7d–e), despite higher viral infection levels in CRH-Cre mice (Fig. 7c), and without affecting locomotion or odor sampling (Supplementary Fig. 7a–b). A previous study found a subtle effect on urination from $Bar^{CRH\text{-}hM4Di}$ inhibition at a much longer 2-hour timescale[15], which we replicated here (Supplementary Fig. 7c) and is consistent with a modulatory role for either Bar^{CRH} or the third population of $Bar^{CRH+ESR1}$ neurons that would be expected to be inhibited with both drivers.

We additionally examined the necessity of Bar^{ESR1} neurons at faster timescales by bilaterally injecting them with AAV-FLEX-ArchT ($Bar^{ESR1\text{-}ArchT}$ mice; Fig. 7f; Supplementary Fig. 8a). We compared urination during 2 minutes of photoinhibition with female odor present to an additional 2 minutes immediately after photoinhibition ceased (Fig. 7g). Sniffing of the female odor did not differ during and after photoinhibition, but urination was largely inhibited during the photoinhibition window (Fig. 7h–j, Supplementary Fig. 8b; Suppl. Video 7). Most trials with female odor, but not with control odor, resulted in urination within seconds of light termination. This suggests that the immediate urine release resulted from priming by odor cues rather than trivial rebound activity upon the cessation of photoinhibition (Fig. 7g–h; Supplementary Fig. 8c). Finally, photoinhibition during cystometry revealed that ongoing Bar^{ESR1} activity is necessary to maintain sphincter bursting, since initiating brief photoinhibition during a reflexive urination event terminated EUS bursting activity and urine release within milliseconds (Supplementary Fig. 8d–e). Together, our experiments indicate that Bar^{ESR1} neurons are essential for urethral inhibition (relaxation) and voluntary urination promoted by olfactory cues in male mice.

Discussion

Bar is well established to be the key conserved brainstem node that coordinates the switch from urine storage to elimination. It is currently modeled as a single projection to the spinal cord that diverges to coordinate both the smooth, involuntary, slow muscle of the bladder wall and the voluntary, striated, fast muscle of the external urethral sphincter (EUS). However, neurons that relax the EUS have not previously been identified, at least in part because voluntary urination is difficult to trigger and study in model organisms. Here we leveraged the natural behavior of male mice, which are highly motivated to scent mark their territory in environments likely to contain females, irrespective of bladder pressure. Our quantitative behavioral assay allowed us to identify and study a novel subpopulation of Bar neurons that are critical to achieve voluntary urination. We further show that optogenetic stimulation of these Bar^{ESR1} neurons in male mice under isoflurane anesthesia can be used as a powerful model of controlled urination. The surprising ability of this minority subset of Bar neurons to drive robust urination comes not from the induced bladder pressure increase, but their unique ability to relax the EUS and gate urine release. It will be of great interest to determine if the function of the Bar^{ESR1} neurons is conserved across evolution since ESR1 expression has also been described in Bar of primates, and human urination similarly depends upon relaxing the urethral sphincter[22,23]. Our findings in mice suggest an updated model of supraspinal urinary control in which Bar sends molecularly and functionally distinct parallel projections to downstream urinary targets (Supplementary Fig. 9a), with

Bar^{ESR1} neurons serving as a key novel subset to enable the study of neural mechanisms underlying voluntary urination.

The majority of neurons in Bar express CRH, yet their anatomy and optogenetic activation indicates a role in focal bladder contraction without relaxing the urethral sphincter. Moreover, chemogenetic inhibition of Bar^{CRH} neurons does not reveal an essential role for this subset of neurons in generating odor-evoked voluntary urination. However, Bar^{CRH} cells have been reported to play a role in urination patterns regulated by long-term social status changes, while CRH itself has a negative effect on urination at longer timescales[20,2,15]. In agreement with these findings, we replicated an earlier finding that inhibition of Bar^{CRH} neurons leads to a modest decrease in urine marks over a much longer two hour assay (Supplementary Fig. 7c)[15]. Additionally, Bar^{CRH} neurons have been proposed to map onto the “direct” subset of Bar neurons whose firing rates correlate directly with reflexive bladder contraction[15], and which some have suggested function to prolong the contraction and maintain appropriate pressure rather than initiate urination[14]. The activity of about one-fourth of Bar neurons does not correlate with reflexive bladder activity at all[14], and our results suggest that urethral inhibition provides another meaningful dimension to Bar categorization. However, a more complete and dynamic catalog of gene expression and spiking activity in Bar neurons during a variety of conditions will likely be needed to fully classify their roles.

Liquid waste elimination is a fundamental animal need, but it must compete with many other potential priorities in a complicated world. These behavioral interactions could explain the need for heterogeneous urination control at the brainstem level, as demonstrated by the actions of Bar^{ESR1} and Bar^{CRH} neurons described here. For example, scent marking to conspecific odor cues is highly sexually dimorphic, but all adult mice additionally urinate under extreme stress[2], analogous to stress incontinence in humans. Mice will also mark more in novel environments[39], and it is well known that urination is modulated by circadian rhythms and fluid homeostasis[40–42]. Finally, control of urination is under complex developmental regulation in rodents, whereby maternal anogenital licking is required in early postnatal life to induce reflex urination and defecation, but this response is later replaced by supraspinal reflexes and even later by voluntary control[1,43]. All of these complications are likely to manifest at one or more levels of the brain, and the separability of Bar subtypes could serve to decouple the actions of bladder and urethra to enable more options for complex control of urination behavior relative to brain state and environment.

Beyond urination, Bar is also implicated in a wider range of pelvic functions (implying that the term “pontine micturition center” is a misnomer[13]) and has recently been termed the ‘pelvic organ stimulating center’ by anatomical and correlational evidence for roles in behaviors such as defecation, sexual behavior, and childbirth, which require varying levels of somatic (e.g. Bar^{ESR1}) and autonomic (e.g. Bar^{CRH}) coordination of the pelvic floor[3,44] (Supplementary Fig. 9b). This multifunctional view of Bar perhaps provides the most parsimonious explanation for molecular, cellular, and physiological heterogeneity in this relatively small nucleus. For example, ejaculation requires striated urethral muscles for semen expulsion, but simultaneous bladder inhibition and backflow prevention[1,45], and likely uses the same pattern generator in the L3-L4 DGC proposed to drive bursting

urination in rodents[30]. The current data shows that Bar^{ESR1} neurons provide input to the DGC at these rostral lumbar levels (Supplementary Fig. 2c) that could drive the expulsion phase of ejaculation, whilst bladder pressure could be independently inhibited. Furthermore, the idea of regulation at different timescales could extend to other pelvic autonomic functions such as pheromone release from the preputial gland, which is also known to be regulated by social status[46] and needs to be synchronized with the urine stream. Other slow functions attributed to the pelvic ganglia, but for which little is known in the central nervous system[47], include sperm production and transport, prostate gland secretions, and various reproductive secretions that differ by species[48,49]. Thus, while the role of Bar^{ESR1} neurons in voluntary urination is clear, our demonstration of functional heterogeneity across Bar invites further study into potential roles for all its neurons in regulating various other pelvic functions.

Incontinence directly or indirectly affects nearly everyone at some point in their life, yet we still have relatively little understanding of how the brain functions or fails to function during this process. Common disruptions include detrusor-sphincter dyssynergia in paraplegics or after spinal cord injury[1], pudendal nerve damage during childbirth, stress urinary incontinence, Fowler's syndrome (inability to voluntarily relax the EUS in women[50]), paruresis (inability to urinate in public), and nocturnal enuresis or bedwetting. Bar^{ESR1} neurons can now serve as an important new target for greater understanding of cause and effect in these disorders. Furthermore, the ability to direct voluntary urination in behaving male mice on a timescale of seconds also opens up new avenues to record and manipulate neural activity during natural urination that is not driven by bladder distension. Bar^{ESR1} neurons form a critical node in this relatively simple and robust social behavior that can be leveraged to rigorously ask how such behavior is modulated by age, sex, state, and learning.

Online Methods

Animals

All animal procedures were conducted in accordance with institutional guidelines and protocols approved by the Institutional Animal Care and Use Committee at The Scripps Research Institute. Mice were group housed at weaning (<5 per cage), single housed for at least 1 week before any testing, and maintained on a 12/12hr light/dark cycle with food and water available ad libitum. All mice were males with a mean age of ~10 weeks when single housed (range 8–12 weeks), and a mean weight of ~27g (range 25–33g). The number of mice used for each experiment is listed below where applicable and in the figure legends. All mouse lines are available at The Jackson Laboratory: CRH-Cre[51] (stock #: 012704), ESR1-Cre[52] (stock #: 017911), Vgat-Cre (stock #: 016962), Vglut2-Cre (stock #: 016963), ROSA-LSL-tdTomato (Ai9, stock #: 007909), ROSA-LSL-ZsGreen (Ai6, stock #: 007906), and BALB/cByJ (stock #: 000651). CRH-Cre and ESR1-Cre mice were backcrossed into the BALB/cByJ background for 3+ generations.

General surgical procedures

Mice were anesthetized with isoflurane (5% induction, 1–2% maintenance, Kent Scientific SomnoSuite) and placed in a stereotaxic frame (David Kopf Instruments Model 962).

Ophthalmic ointment (Puralube) was applied, buprenorphine (Buprenex, 0.15mg/kg) was administered intramuscularly at the beginning of the procedure, and 500uL sterile saline containing carprofen (Rimadyl, 5mg/kg) and enrofloxacin (Baytril, 5mg/kg) was administered subcutaneously at the end of the procedure. Mice were monitored daily and given at least 14 days for recovery and viral expression before subsequent behavioral testing.

AAV viral vectors

For photostimulation, AAV9-CAG-FLEX-ChR2-tdTomato (UPenn AV-9-18917P) was injected bilaterally at 1.4×10^{12} GC/mL in both ESR1-Cre and CRH-Cre animals. For CRH-Cre animals only, we also included AAV1-EF1α-FLEX-hChR2-eYFP (1:1 mix with above, UPenn AV-1-20298P) since this virus expressed at higher levels in Bar^{CRH} neurons in preliminary experiments. For photostimulation controls, AAV9-CAG-FLEX-GFP (UNC AV5220) was injected bilaterally at 3.2×10^{13} GC/mL in ESR1-Cre mice. For ESR1-Cre DREADD inhibition[53], AAVdj-CAG-FLEX-hM4Di-GFP[54] (Addgene plasmid # 52536, a gift from Scott Sternson) was produced by the Salk Institute Gene Transfer Targeting and Therapeutics Core (GT3) and injected bilaterally at 8×10^{12} GC/mL. We did not see efficient expression using this virus in CRH-Cre animals, so for CRH-Cre DREADD inhibition, AAVdj/1-EF1α-FLEX-hM4Di-mCherry (Addgene plasmid # 50461, a gift from Bryan Roth) was produced by Virovek and injected bilaterally at 4×10^{12} GC/mL. For photoinhibition, AAV9-CAG-FLEX-ArchT-GFP (UNC AV6222) was injected bilaterally at 2.2×10^{12} GC/mL in ESR1-Cre animals, and the same virus and titer were used for anatomical axon tracing unilaterally in both ESR1-Cre and CRH-Cre animals. For fiber photometry, AAV-CAG-FLEX-GCaMP6s[55] (UPenn AV-9-PV2818) was unilaterally injected at 3.2×10^{12} GC/mL in ESR1-Cre animals.

Viral injection and fiber optic implantation

Injections were made using pulled glass pipettes (tips broken for ID = 10–20μm) and a Picospritzer at 25 – 75 nL/min. For Bar injections, the overlying muscle was removed and a medial-lateral angle of 33° was used to avoid the 4^{th} ventricle. The pipette entry coordinate relative to bregma was 5.3mm caudal, 2.5mm lateral, and 3.2mm diagonally below the dura. The surrounding skull area was thinned for visualization with a diamond drill bit and the rostral-caudal coordinate was adjusted if necessary to coincide with the junction of the inferior colliculus and cerebellum, and to avoid hitting the transverse sinus. AAVs were injected 30–150nL per side, and the pipette was left in place for 5 min after injection, before slowly retracting. Fiber optic implants (4 mm length, Plexon 230μm diameter for ChR2/ArchT and Doric 400μm diameter for GCaMP) were inserted along the pipette track as above, 300μm above the injection site for ChR2/ArchT, and 50μm for GCaMP. Additionally, two anchor screws (Antrin Miniature Specialties M1 X .060″) were attached over frontal cortex for animals with implants. After injection/implantation, the skull was covered with superglue and dental cement to seal the craniotomy and hold the implants in place.

Spinal cord CTB injection

A 1–2 cm incision was made over lumbar segments, and the connective tissue and muscle overlying the vertebrae was minimally dissected[56] to expose L1 and L2 vertebrae[57]. Vertebrae and underlying spinal segments were located by spinous process tendon

attachments and spinous process shape, and confirmed by pilot injections of DiD dye. A spinal adapter[56] for the stereotaxic frame (Stoelting 51690) was used to clamp L2 transverse processes, and a beveled glass pipette was lowered into the space between L1 and L2 vertebrae, 400μm lateral to the spinous process midline and 600μm below dura, to target the sacral mediolateral column bladder preganglionic neurons. After injection of 150 nL CTB-488 (ThermoFisher, 0.5% in PBS), the pipette was left in place for 5 min before slowly retracting, and then the injection site was covered with gelfoam and the overlying skin was sutured. Survival time was 5 days.

Odor-motivated urination assay

Sexually naïve male mice were briefly prescreened for urination responses to 100uL female urine (>1 second odor sampling period with >3 urine marks within 1 minute) before any further testing or manipulation, which excluded 21% of all mice tested. The remaining 79% had surgical procedures and recovery or a 2 week waiting period before starting habituation. Mice were habituated in the behavior room for 3 consecutive days, for 16/8/4 minute durations on days 1/2/3. On day 3, control stimuli (100uL tonic water, which fluoresces under UV illumination) were pipetted from above at 0 min. and 2 min. and the baseline response was recorded. On subsequent test days, a 4 min. assay was used, with 100uL tonic water delivered at 0 minutes and 100uL female urine delivered at 2 min. All behavior was conducted during light hours under dim red light, and 70% ethanol was used to clean equipment between trials. The recording box consisted of a UV-opaque acryllic homecage with the bottom cut out, placed on top of 0.35mm chromatography paper (Fisher Scientific 05-714-4) resting on clear glass (Supplementary Fig. 4a). Two wide angle cameras (Logitech C930e), one above on a modified cage top, and one below the bottom glass, streamed video to a laptop computer at 15 frames per second, 640×360 pixel resolution. An analog pulse controlled LEDs in each camera field of view in order to synchronize cameras. Two UV fluorescent tube lights (American DJ Black-24BLB) surrounded by foil walls were used to evenly illuminate the chromatography paper from below. Videos were cut using Adobe After Effects and subsequently analyzed for urine marks using custom MATLAB software. The red and green channels of the RGB camera frames were used for urine detection, and the blue channel for mouse tracking. An output video with urine detection overlay was generated to manually verify automatic spot detection. Noldus Ethovision XT was used to automatically track mice and determine distance traveled and odor sniffing periods, defined as when the nosepoint occluded the female urine stimulus.

Female urine collection

Adult (8–16 weeks) C57BL/6N female mice were housed 5 per cage, soiled male bedding was introduced into the cage 24 hours before the first collection night to induce estrous, and urine was pooled from 4 cages (20 mice total) over 4 days such that the stimulus consisted of a mix from all stages of the estrous cycle[58]. The mice were placed in metabolic cage for 12–16 hours at a time overnight, and urine was collected directly into a sterile tube on dry ice[59] and temporarily stored at −20°C in the morning. After 4 consecutive nights of collection, urine was thawed on ice, rapidly passed through a 0.22μm filter (Millipore Steriflip SCGP00525) before aliquoting and storing at −80°C. Two different batches of urine

were collected for all experiments, and each was used with both control and experimental groups.

Chemogenetic inhibition

After hM4Di[53] viral injection, mice were allowed at least 21 days for recovery and expression, and then intraperitoneally injected 45–55 minutes before testing with either control saline plus 0.5% DMSO, or Clozapine N-oxide (CNO, 5mg/kg, Enzo Life Sciences BML-NS105-0025) in saline plus 0.5% DMSO. Control saline injections were performed on the 3 habituation days before female urine was given. Then on days 4/5/6/7, mice received CNO/saline/CNO/saline before the female urine countermarking assay described above. CRH-Cre mice were tested for 2 additional days (CNO, then saline) using the same assay but with 2-hour duration. Mice with less than 3 marks within 2 minutes after stimulus on both saline control days were excluded from analysis (8 of 34 mice), as well as mice that did not have bilateral hM4Di expression that spanned at least ±100μm from the Bar rostral-caudal center, defined by ovoid Nissl clustering medial to locus coeruleus (7 of 34 mice). The “CNO Urine Inhibition Index” (CUI) was calculated as [(fraction max. urine marks on saline days) - (fraction max. urine marks on CNO days)], such that CUI = 2 represents complete inhibition by CNO relative to saline, while CUI = 0 represents no difference between saline and CNO days.

Optogenetic stimulation

For photostimulation experiments, fiber-implanted mice were briefly anesthetized with 5 % isoflurane before connecting and disconnecting patch cables (Plexon 0.5m, 230μm diameter). An LED current source (Mightex BLS-SA02-US) driving two 465nm PlexBright Compact LED Modules (Plexon) through a Dual LED Commutator (Plexon) provided 10±1 mW exiting the fiber tips. Optical power was measured (ThorLabs PM20A) before and after each session. Mice were placed in the same recording box described above for behavior, but with thinner 0.19 mm chromatography paper (Fisher Scientific 05-714-1). Initial experiments with different pulse widths determined 15 msec to be more effective than 5 msec or 1 msec at driving urination responses. All photostimulation bouts occurred for 5 sec duration using 15 msec pulses at five different frequencies: 1, 5, 10, 25, and 50Hz. These frequencies were stimulated in increasing order on the first day, and then repeated in decreasing order on the second day. At least 1 min elapsed between different photostimulation bouts, with additional delays occasionally necessary to allow the mouse to move to a clean section of paper. Videos were cut using Adobe After Effects (version CS5) and subsequently analyzed for urine marks using custom MATLAB software (version 2014b). Urine amount was calculated from urinated pixels detected using second-order polynomial coefficients determined with MATLAB *polyfit* on male urine calibration data (Supplementary Fig. 3c–d). Response latency was calculated as the earliest point when the normalized Δurine derivative reached 10% of maximum during the 15 sec response period. For a subset of mice, we repeated photostimulation on a third day under 1.5% maintenance isoflurane anesthesia. Four anesthetized 50 Hz/15 msec/5 sec photostimulation bouts separated by 1 min/1 min/1 min/5 min were conducted, then the isoflurane was removed and the mouse was allowed to recover to walking before waiting 5 min and following with two awake 50 Hz/15 msec/5 sec bouts separated by 1 min/5 min to confirm that awake urination

was intact. After all experiments, mice were perfused and checked for viral expression and fiber placement as described for immunohistochemistry. Mice that did not have at least unilateral ChR2 expression that spanned ±100μm from the Bar rostral-caudal center were excluded from analysis (9 of 29 mice).

Optogenetic inhibition

For photoinhibition, all procedures were same as for photostimulation described above except for the following changes: fiber implanted mice were not anesthetized before connecting patch cables, but were habituated to the procedure for at least 3 days before testing. On the final habituation day, control odor was presented and 3 different photoinhibition periods were applied (2x 30 sec., 1x 2 min., separated by at least 30 seconds) to test the baseline effects of ArchT inhibition on urine output. Plexon 550 nm PlexBright Compact LED Modules were used, providing provided 6±1 mW exiting the fiber tips. During odor-motivated urination assay as described above, 2 min. of constant photoinhibition was applied 105 seconds after control odor, and 10–15 seconds before female urine. Urine marking behavior continued for 2 min. after photoinhibition ceased. Mice that did not have bilateral ArchT expression that spanned ±100μm from the Bar rostral-caudal center were excluded from analysis (7 of 10 mice).

Fiber photometry

Bulk GCaMP fluorescence was collected at 20 Hz using a similar setup to that previously described[60]. ΔF/F was calculated as (F – median(F)/median(F)) for each trial. An analog pulse controlled LEDs in each camera field of view as well as an Arduino sending triggers to the sCMOS camera (Hamamatsu ORCA-Flash4), in order to synchronize video and GCaMP data streams. Mice were recorded for 8 min. total (4 min. control odor only, then 4 min. with female urine stimulus). Δurine peaks were calculated from bottom video (MATLAB *findpeaks* function) with a minimum peak of 0.18 μL/frame, and GCaMP traces were analyzed around these peaks (zero lag) or at randomly selected times within the same assay (shuffle lag) as a control. The MATLAB *corrcoef* function was used to calculate correlation between GCaMP and Δurine traces.

Electromyography and cystometry

Fiber-implanted mice were anesthetized with isoflurane (5% induction, 2% maintenance) and the bladder and external urethral sphincter (EUS, or urethral rhabdosphincter)[61,62] were exposed via ~1cm midline abdominal incision. Flanged PE20 tubing connected to a syringe pump and pressure sensor (Biopac Systems DA100C/TSD104A) using a 25G needle was inserted and sutured into the bladder dome. Two tungsten wires (A-M Systems 795500) were stripped of insulation 1–2mm at the ends and inserted bilaterally (~2mm separation) into the EUS just proximal to the pubic symphysis, using a 30G needle. A third ground wire was stripped 3–4mm at the end and placed subcutaneously. The abdominal incision was sutured, allowing the tubing and wires to exit and connect to a differential amplifier (Biopac Systems EMG100C: gain = 5000, sample rate = 10kHz, low pass filter = 5kHz, 60Hz notch filter and 100Hz high pass filter). A digital input was simultaneously acquired at 10kHz, which was controlled by a TTL switch that also triggered optogenetic stimulation. After suturing, isoflurane was reduced to 1.0–1.8% (minimal to eliminate movement artifacts) and

the bladder was filled at 10–20μL/min for at least 45 min. before starting photostimulation. Once a regular rhythm of urination cycles was established, the volume threshold was calculated as the mean volume of 3 cycles, and “filled” and “empty” states were defined as 75% and 10% of this mean value. Only mice with natural bursting cycles were analyzed for photostimulated or photoinhibited responses. Photostimulation consisted of 50 Hz/15 msec/5 sec photostimulation bouts separated by > 1 min. Photoinhibition consisted of constant illumination for 2 or 5 seconds, manually triggered at the beginning of a burst event. Root-mean-square (RMS) EMG traces were calculated using a 300 msec Gaussian filter and subtraction of the mean across 5 seconds prior to photostimulation. Sphincter relaxation periods were defined using RMS EMG data as periods between peaks >0.1mV (MATLAB *findpeaks* function) with amplitude less than the mean value prior to photostimulation. Frequency content of RMS EMG traces was calculated by first downsampling to 200 Hz, and then taking the FFT in overlapping 2 sec. rectangular windows. The spectrogram was thresholded at −40dB and burst duration was calculated as the time in which mean power in the 5–15Hz band is above this threshold.

Wireless corpus spongiosum recording

Wireless pressure sensors (Data Sciences International, DSI PA-C10) were sterilized and implanted in the bulb of the corpus spongiosum that surrounds the urethra as previously described[38,63,64], with the transmitter placed subcutaneously in the lateral abdominal area. After 1 week recovery, mice were recorded in the odor-motivated urine assay as described above, but with a single camera and UV illumination from above and the DSI RPC-1 receiver below the test cage. Pressure data was logged at 500 Hz and synchronized to urine imaging video. Frequency content of pressure traces was calculated by taking the FFT in overlapping 2 sec. hamming windows.

Slice electrophysiology

Mice were deeply anesthetized with isoflurane, and acute 300μm coronal brain sections were prepared after intracardial perfusion of ice-cold choline-based slicing solution containing (in mM): 25 $NaHCO_3$, 1.25 NaH_2PO_4, 2.5 KCl, 7 $MgCl_2$, 25 glucose, 0.5 $CaCl_2$, 110 choline chloride, 11.6 sodium ascorbate, 3.1 sodium pyruvate). Brains were quickly transferred and sliced in the same solution with a vibratome (LeicaVT1200). Sections were transferred to a recovery chamber and incubated for 15–20 min at 35 °C in recovery solution consisting of (in mM): 118 NaCl, 2.6 $NaHCO_3$, 11 glucose, 15 HEPES, 2.5 KCl, 1.25 NaH_2PO_4, 2 sodium pyruvate, 0.4 sodium ascorbate, 2 CaCl2, 1 MgCl2. Slices were maintained at room temperature for at least 30 min until transferred to bath for recording. Cutting solution, recovery solution, and ACSF were constantly bubbled with 95% O_2/5% CO_2. Slices were transferred to a recording chamber on an upright fluorescent microscope continuously perfused with oxygenated ACSF (in mM):125 NaCl, 25 $NaHCO_3$, 2.5 KCl, 1.25 NaH_2PO_4, 11 glucose, 1.3 $MgCl_2$ and 2.5 $CaCl_2$ at 28–31 °C using a feedback temperature controller. Neurons labeled by fluorescent markers were visualized with a 40X water-immersion objective with epifluorescence and infrared differential interference contrast video microscopy. Recording pipettes were pulled from borosilicate glass (G150TF-4; Warner Instruments) with 3–5 MΩ resistance. The internal solution for current-clamp recording consisted of the following (in mM): 125 potassium D-gluconate, 4 NaCl, 10 HEPES, 0.5

EGTA, 20 KCl, 4 Mg_2-ATP, 0.3 Na_3-GTP, and 10 phosphocreatine. Recordings were made using a MultiClamp700B amplifier and pClamp software (Molecular Devices). The signal was low-pass filtered at 1 kHz and digitized at 10 kHz with a digitizer (Molecular Devices). For photostimulation of ChR2, 15 ms/5 sec duration blue light pulses were emitted from a collimated light-emitting diode (473 nm; Thorlabs) driven by a T-Cube LED Driver (Thorlabs) under the control of a Digidata 1440A Data Acquisition System and pClamp software. Light was delivered through the reflected light fluorescence illuminator port and the 40X objective (light power at max setting measured at 13.45 mW). Analysis was performed in either Clampfit (Molecular Devices) or OriginPro 2016 (Origin Lab).

Immunostaining

Animals were perfused with cold PBS followed by 4% PFA, and the brain/spinal cord (SC) was dissected and postfixed in 4% PFA at 4°C for 24–48 hours. The brain/SC was then washed in PBS and embedded in 1% low melting point agarose and cut on a vibratome at 50μm for ESR1 staining or 100μm for Nissl-only staining. Spinal cords were cut transversely across the entire thoracolumbar and lumbosacral region and matched to segments using Nissl landmarks. For ESR1 immunostaining, free-floating sections were blocked in 1% BSA (Sigma A3059) in 1% PBST (PBS plus Triton X-100) for 3 hours, followed by primary incubation with anti-ESR1 antibody[17,52,65] (antigen is mouse C-terminus fragment; Santa Cruz sc-542, rabbit polyclonal, 100μg/mL diluted 1:500 in 1% BSA/0.3% PBST) overnight at room temperature. Sections were washed 3X with 0.1% PBST and blocked again at room temperature for 1 hour, before incubating in secondary antibody (ThermoFisher Alexa-Fluor 488 or 647 anti-rabbit IgG H+L diluted 1:2000 in 1% BSA/0.3% PBST) at room temperature for 3 hours. Nissl stain (ThermoFisher NeuroTrace Blue or Deep Red diluted 1:200) was also included here if necessary, or incubated for 2 hours in 0.3% PBST if used alone. Sections were washed 2X in 0.1% PBST followed by 2X PBS, then mounted with ProLong Diamond (ThermoFisher).

Fluorescent in situ hybridization

Mice were anesthetized with isoflurane before rapid brain extraction, embedding in OCT, and freezing on dry ice. Coronal sections were cut at 20μm and stored at −80°C until processing according to the protocol provided in the RNAscope® Multiplex Fluorescent v2 kit (Advanced Cell Diagnostics). Sections were fixed in 4% PFA, dehydrated, and hybridized with mixed probes: *Crh* (Mm-crh, Cat. 316091), *Esr1* (Mm-Esr1-O2-C2, a 16ZZ probe targeting 1308-2125 of NM_007956.5.), *Slc32a1* (*Vgat*, Mm-Slc32a1, Cat. 319191), and *Slc17a6 (Vglut2*, Mm-Slc17a6-C2, Cat. 319171) for 2h at 40°C and followed by amplification. Signal in each channel is developed using TSA Cyanine 3, fluorescein, and Cyanine 5 (PerkinElmer) individually. Sections were counterstained with DAPI and mounted with ProLong Diamond.

Confocal Microscopy

Images were captured with Nikon A1 Confocal Microscope with a 10x air, 20x air or 40x oil objective. Nikon Elements software settings were optimized for each experiment to maximize signal range, and z-stack maximum projections were used for representative images and axonal projections while single optical slices were used for quantification of cell

body overlap. For RNAScope, z-stacks were collected in 1μm increments throughout the z-axis.

Anatomical quantification

The rostrocaudal center of Bar was defined as two consecutive 50μm section with greatest ESR1 and CRH-tdT labelling whenever possible, or by distinctive ovoid Nissl boundaries. Custom MATLAB scripts were used to draw ROIs around Bar and semi-automatically count cells with clear cell body staining. Cells with high expression of ESR1 were distinguished from background labeling by thresholding in the ESR1 color channel just below the mean intensity level of nearby parabrachial neurons with established strong ESR1 expression[29,66]. Cartesian coordinates for cell locations were saved and the centroid of CRH-tdT cells was used to register different sections to generate the overlay plot in Fig. 1d and Supplementary Fig. 9. For calculation of fluorescence intensity ratio (Fig. 1k) in the lumbosacral mediolateral column (ML) and dorsal grey commissure (DGC), all intact L5-S2 sections with visible axons were used. A rectangular ROI was drawn using the Nissl color channel to encapsulate the MLs and area in between. This ROI was then equally divided into medial-lateral thirds and the Bar axon color channel was used to calculate the sum of pixel intensity across each third. The ratio was calculated as this total pixel intensity in the middle DGC third divided by that of the 2 ML thirds averaged together.

Statistics and reproducibility

Nonparametric tests were used for all experiments, as detailed in the figure legends, which do not make assumptions about data distributions or variances. The Wilcoxon signed rank test (MATLAB *signrank*) was used for comparison of 2 paired groups, and the Mann-Whitney U test (aka. Wilcoxon rank sum test; MATLAB *ranksum*) for 2 unpaired groups. Friedman's test (MATLAB *friedman*) was used to compare across CNO and saline treatments for 4-day DREADD experiments, followed by Dunn-Sidak posthoc tests (MATLAB *multcompare*). Points with error bars represent mean ± s.e.m.

For most experiments, no statistical methods were used to pre-determine sample sizes but our sample sizes are similar to those reported in previous publications[52–54]. We used the effect size from preliminary wild-type chemogenetic experiments to calculate sample sizes for ESR1-Cre and CRH-Cre chemogenetic experiments (Fig. 7d–e), using the *sampsizepwr* function in MATLAB. For each experiment, animals were maintained under identical conditions, such that no randomization was used to assign groups. Data collection and analysis were generally not performed blind to the conditions of the experiments. However, automated data analysis in MATLAB and Ethovision was used to track animal behavior such that no blinding is necessary to ensure behavioral data integrity. Semi-automated analyses similarly assisted cell counting, where the Nissl channel was used to manually define the Bar region-of-interest, rather than the cell-counting channel.

In Fig. 1b–c, Bar sections from n=6 mice were imaged, shown together in Fig. 1d–f. In Fig. 1g–I, injection sites and lumbosacral spinal cords from n=5 unitateral AAV-FLEX-GFP injection animals and n=5 bilateral AAV-FLEX-ChR2 animals were used (10 total each, for ESR1-Cre and CRH-Cre lines) with similar results to calculate the total summary in Fig. 1l.

In Fig. 2a–c, fiber photometry with video recording and injection site imaging was recorded in n=7 mice with similar results. In Fig. 3b, n=10 mice were imaged with similar injection sites in both ESR1-Cre and CRH-Cre lines, as quantified in Fig. 3c. In Fig. 4b, cystometry recordings were repeated in n=3 ESR1-Cre mice and n=5 CRH-Cre mice, similar to examples shown. In Fig. 5c, EMG recordings were repeated in n=6 ESR1-Cre mice and n=5 CRH-Cre mice, similar to examples shown. In Fig. 6a, scent marking behavior was repeated in n=12 wild-type mice with similar results. In Fig. 7a–b, scent marking behavior with chemogenetic inhibition and imaging of injection sites was repeated in n=8 ESR1-Cre mice and n=10 CRH-Cre mice with similar results. In Suppl. Fig. 1a–c, similar results were obtained in n=3 ESR1-ZsGreen, n=4 Vgat-ZsGreen, and n=3 Vglut2-ZsGreen reporter mice. In Suppl. Fig. 1d–k, similar RnaScope in-situ hybridization results were obtained in n=5 mice for each probe combination. In Suppl. Fig. 1m–n, similar CTB tracing results were obtained in n=2 mice. In Suppl. Fig. 2b–c, injection sites and lumbosacral spinal cords from n=5 unitateral AAV-FLEX-ArchT-GFP injection animals and n=5 bilateral AAV-FLEX-ChR2 animals were used (10 total each, for ESR1-Cre and CRH-Cre lines), as in Fig. 1g–i but with different example animals shown. For Suppl. Fig. 3b, similar video recordings were made for all optogenetic, chemogenetic, and fiber photometry experiments reported here. In Suppl. Fig. 4a–b, patch clamp recordings were repeated with similar results in n=6 $Bar^{CRH\text{-}ChR2}$ neurons from 2 mice, n=12 $Bar^{ESR1\text{-}ChR2}$ neurons from 3 mice, and n=4 $Bar^{ESR1\text{-}GFP}$ neurons from 2 mice. In Suppl. Fig. 5b, the data were repeated with similar results in 33 trials across 6 mice as summarized in Fig. 5b, e (top). In Suppl. Fig. 5c–f, wireless corpus spongiosum recordings were repeated in n=2 mice with similar results. In Suppl. Fig. 6, $Bar^{ESR1\text{-}ChR2}$ stimulation during cystometry was repeated in the empty bladder condition for 45 trials across 6 mice, with about half showing similar weak burst responses as shown in Fig. 5b. In Suppl. Fig. 8a, $Bar^{ESR1\text{-}ArchT}$ expression was similar in n=3 bilaterally infected mice. In Suppl. Fig. 8d, $Bar^{ESR1\text{-}ArchT}$ similarly inhibited ongoing reflexive bursting in n=5 trials across 2 animals, as shown in Suppl. Fig. 8e.

Code availability

Custom MATLAB scripts were used to analyze and plot all data. The main analysis code was used for automated urine detection from raw video data, as detailed in Suppl. Fig. 3. The same code was used for all behavior data and is available in the Supplementary Software file or online at: github.com/stowerslab/smuf.

Data availability

The data that support the findings of this study are available from the corresponding author upon reasonable request.

Accession codes

There are no accession codes for this manuscript.

Life Sciences Reporting Summary

Further information is available in the Life Sciences Reporting Summary.

Supplementary Material

Refer to Web version on PubMed Central for supplementary material.

Acknowledgments

We thank W. de Groat for constructive comments and discussions on an earlier version of the manuscript, and S. Mukhopadhyay for help with behavior. J.A.K. was supported by NSF-GRFP grant DGE-1144086. L.S is funded by NSF IOS-1556085 and NIH R01-DC015253.

References

1. de Groat WC, Griffiths D, Yoshimura N. Neural Control of the Lower Urinary Tract. In: Terjung R, editorComprehensive Physiology. John Wiley & Sons, Inc; 2014. 327–396.
2. Valentino RJ, Wood SK, Wein AJ, Zderic SA. The bladder–brain connection: putative role of corticotropin-releasing factor. Nat Rev Urol. 2011; 8:19–28. [PubMed: 21135878]
3. Holstege G. The emotional motor system and micturition control. Neurourol Urodyn. 2010; 29:42–48. [PubMed: 20025036]
4. Minassian VA, Drutz HP, Al-Badr A. Urinary incontinence as a worldwide problem. Int J Gynecol Obstet. 2003; 82:327–338.
5. Bayani D-M, Taborsky M, Frommen JG. To pee or not to pee: urine signals mediate aggressive interactions in the cooperatively breeding cichlid Neolamprologus pulcher. Behav Ecol Sociobiol. 2017; 71
6. Reynolds E. Urination as a Social Response in Mice. Nature. 1971; 234:481–483. [PubMed: 4944197]
7. Hurst JL, Beynon RJ. Scent wars: the chemobiology of competitive signalling in mice. BioEssays. 2004; 26:1288–1298. [PubMed: 15551272]
8. Heymann EW. Scent marking strategies of new world primates. Am J Primatol. 2006; 68:650–661. [PubMed: 16715511]
9. Gosling LM, Roberts SC, Thornton EA, Andrew MJ. Life history costs of olfactory status signalling in mice. Behav Ecol Sociobiol. 2000; 48:328–332.
10. Desjardins C, Maruniak JA, Bronson FH. Social Rank in House Mice: Differentiation Revealed by Ultraviolet Visualization of Urinary Marking Patterns. Science. 1973; 182:939–941. [PubMed: 4745598]
11. Roberts SC, Gosling LM, Thornton EA, McClung J. Scent-marking by male mice under the risk of predation. Behav Ecol. 2001; 12:698–705.
12. Barrington FJF. The effect of lesions of the hind- and mid-brain on micturition in the cat. Q J Exp Physiol. 1925; 15:81–102.
13. Verstegen AMJ, Vanderhorst V, Gray PA, Zeidel ML, Geerling JC. Barrington's nucleus: Neuroanatomic landscape of the mouse "pontine micturition center". J Comp Neurol. 2017; 525:2287–2309. [PubMed: 28340519]
14. Sasaki M. Role of Barrington's nucleus in micturition. J Comp Neurol. 2005; 493:21–26. [PubMed: 16255005]
15. Hou XH, et al. Central Control Circuit for Context-Dependent Micturition. Cell. 2016; 167:73–86.e12. [PubMed: 27662084]
16. Sutin EL, Jacobowitz DM. Immunocytochemical localization of peptides and other neurochemicals in the rat laterodorsal tegmental nucleus and adjacent area. J Comp Neurol. 1988; 270:243–270. [PubMed: 2897981]
17. VanderHorst VGJM, Gustafsson J-Å, Ulfhake B. Estrogen receptor-α and -β immunoreactive neurons in the brainstem and spinal cord of male and female mice: Relationships to monoaminergic, cholinergic, and spinal projection systems. J Comp Neurol. 2005; 488:152–179. [PubMed: 15924341]

18. Vincent SR, Satoh K. Corticotropin-releasing factor (CRF) immunoreactivity in the dorsolateral pontine tegmentum: further studies on the micturition reflex system. Brain Res. 1984; 308:387–391. [PubMed: 6383518]
19. Valentino RJ, Pavcovich LA, Hirata H. Evidence for corticotropin-releasing hormone projections from Barrington's nucleus to the periaqueductal gray and dorsal motor nucleus of the vagus in the rat. J Comp Neurol. 1995; 363:402–422. [PubMed: 8847408]
20. McFadden K, Griffin TA, Levy V, Wolfe JH, Valentino RJ. Overexpression of corticotropin-releasing factor in Barrington's nucleus neurons by adeno-associated viral transduction: effects on bladder function and behavior. Eur J Neurosci. 2012; 36:3356–3364. [PubMed: 22882375]
21. Rouzade-Dominguez ML, Pernar L, Beck S, Valentino RJ. Convergent responses of Barrington's nucleus neurons to pelvic visceral stimuli in the rat: a juxtacellular labelling study. Eur J Neurosci. 2003; 18:3325–3334. [PubMed: 14686905]
22. Tanagho EA, Miller ER. Initiation of voiding. Br J Urol. 1970; 42:175–183. [PubMed: 5420157]
23. Yalla SV, Resnick NM. Initiation of Voiding in Humans: The Nature and Temporal Relationship of Urethral Sphincter Responses. J Urol. 1997; 157:590–595. [PubMed: 8996365]
24. Blok BF, van Maarseveen JT, Holstege G. Electrical stimulation of the sacral dorsal gray commissure evokes relaxation of the external urethral sphincter in the cat. Neurosci Lett. 1998; 249:68–70. [PubMed: 9672391]
25. Grill WM, Bhadra N, Wang B. Bladder and urethral pressures evoked by microstimulation of the sacral spinal cord in cats. Brain Res. 1999; 836:19–30. [PubMed: 10415401]
26. Shefchyk SJ. Sacral spinal interneurones and the control of urinary bladder and urethral striated sphincter muscle function. J Physiol. 2001; 533:57–63. [PubMed: 11351013]
27. Kruse MN, Noto H, Roppolo JR, de Groat WC. Pontine control of the urinary bladder and external urethral sphincter in the rat. Brain Res. 1990; 532:182–190. [PubMed: 2282512]
28. Mallory BS, Roppolo JR, de Groat WC. Pharmacological modulation of the pontine micturition center. Brain Res. 1991; 546:310–320. [PubMed: 1676929]
29. VanderHorst VGJM, Terasawa E, Ralston HJ. Estrogen receptor-α immunoreactive neurons in the brainstem and spinal cord of the female rhesus monkey: Species-specific characteristics. Neuroscience. 2009; 158:798–810. [PubMed: 18996446]
30. Chang HY, Cheng CL, Chen JJJ, de Groat WC. Serotonergic drugs and spinal cord transections indicate that different spinal circuits are involved in external urethral sphincter activity in rats. AJP Ren Physiol. 2006; 292:F1044–F1053.
31. Kaur AW, et al. Murine Pheromone Proteins Constitute a Context-Dependent Combinatorial Code Governing Multiple Social Behaviors. Cell. 2014; 157:676–688. [PubMed: 24766811]
32. Chang HY, Havton LA. Differential effects of urethane and isoflurane on external urethral sphincter electromyography and cystometry in rats. AJP Ren Physiol. 2008; 295:F1248–F1253.
33. Smith PP, DeAngelis AM, Kuchel GA. Evidence of central modulation of bladder compliance during filling phase. Neurourol Urodyn. 2012; 31:30–35. [PubMed: 22038779]
34. le Feber J, van Asselt E. Pudendal nerve stimulation induces urethral contraction and relaxation. Am J Physiol-Regul Integr Comp Physiol. 1999; 277:R1368–R1375.
35. Cruz Y, Downie JW. Sexually dimorphic micturition in rats: relationship of perineal muscle activity to voiding pattern. Am J Physiol-Regul Integr Comp Physiol. 2005; 289:R1307–R1318. [PubMed: 15994373]
36. LaPallo BK, Wolpaw JR, Chen XY, Carp JS. Contribution of the external urethral sphincter to urinary void size in unanesthetized unrestrained rats. Neurourol Urodyn. 2015
37. Kadekawa K, et al. Characterization of bladder and external urethral activity in mice with or without spinal cord injury - a comparison study with rats. Am J Physiol - Regul Integr Comp Physiol. 2016; 310:R752–R758. [PubMed: 26818058]
38. Nout YS, et al. Novel technique for monitoring micturition and sexual function in male rats using telemetry. Am J Physiol-Regul Integr Comp Physiol. 2007; 292:R1359–R1367. [PubMed: 17095649]
39. Matthews MK. Urinary marking and tendency to investigate novelty in Mus musculus. Behav Neural Biol. 1980; 28:501–506. [PubMed: 7406808]

40. Maruniak JA, Taylor JA, Perrigo G. Effects of Water Deprivation on Urine Marking and Aggression in Male House Mice. Physiol Behav. 1988; 42:47–51. [PubMed: 3387476]
41. Ogier R, Tribollet E, Suarez P, Raggenbass M. Identified Motoneurons Involved in Sexual and Eliminative Functions in the Rat Are Powerfully Excited by Vasopressin and Tachykinins. J Neurosci. 2006; 26:10717–10726. [PubMed: 17050711]
42. Ueno H, Kuno M, Shintani Y, Kamo I. Role of vasopressin V1A receptor in the urethral closure reflex in rats. Am J Physiol-Ren Physiol. 2011; 300:F976–F982.
43. Moore CL. The Role of Maternal Stimulation in the Development of Sexual Behavior and Its Neural Basis. Ann N Y Acad Sci. 1992; 662:160–177. [PubMed: 1456637]
44. Holstege G. How the Emotional Motor System Controls the Pelvic Organs. Sex Med Rev. 2016; 4:303–328. [PubMed: 27872027]
45. Veening JG, Coolen LM. Neural mechanisms of sexual behavior in the male rat: Emphasis on ejaculation-related circuits. Pharmacol Biochem Behav. 2014; 121:170–183. [PubMed: 24368305]
46. Barnett SA, Dickson RG, Warth KG. Social status, activity and preputial glands of wild and domestic house mice. Zool J Linn Soc. 1980; 70:421–430.
47. Keast JR. Unusual Autonomic Ganglia: Connections, Chemistry, and Plasticity of Pelvic Ganglia. Int Rev Cytol. 1999; 193:1–69. [PubMed: 10494620]
48. Wanigasekara Y, Kepper ME, Keast JR. Immunohistochemical characterisation of pelvic autonomic ganglia in male mice. Cell Tissue Res. 2003; 311:175–185. [PubMed: 12596037]
49. Bartlett MJ, Steeves TE, Gemmell NJ, Rosengrave PC. Sperm competition risk drives rapid ejaculate adjustments mediated by seminal fluid. eLife. 2017; 6:e28811. [PubMed: 29084621]
50. Osman NI, Chapple CR. Fowler's syndrome - a cause of unexplained urinary retention in young women? Nat Rev Urol. 2014; 11:87–98. [PubMed: 24323131]
51. Taniguchi H, et al. A Resource of Cre Driver Lines for Genetic Targeting of GABAergic Neurons in Cerebral Cortex. Neuron. 2011; 71:995–1013. [PubMed: 21943598]
52. Lee H, et al. Scalable control of mounting and attack by Esr1+ neurons in the ventromedial hypothalamus. Nature. 2014; 509:627–632. [PubMed: 24739975]
53. Krashes MJ, et al. Rapid, reversible activation of AgRP neurons drives feeding behavior in mice. J Clin Invest. 2011; 121:1424–1428. [PubMed: 21364278]
54. Atasoy D, Betley JN, Su HH, Sternson SM. Deconstruction of a neural circuit for hunger. Nature. 2012; 488:172–177. [PubMed: 22801496]
55. Chen TW, et al. Ultrasensitive fluorescent proteins for imaging neuronal activity. Nature. 2013; 499:295–300. [PubMed: 23868258]
56. Cunningham MG, Donalds RA, Scouten CW, Tresch MC. A versatile, low-cost adaptor for stereotaxic and electrophysiologic spinal preparations in juvenile and adult rodents. Brain Res Bull. 2005; 68:157–162. [PubMed: 16325015]
57. Harrison M, et al. Vertebral landmarks for the identification of spinal cord segments in the mouse. NeuroImage. 2013; 68:22–29. [PubMed: 23246856]
58. Holy TE, Dulac C, Meister M. Responses of Vomeronasal Neurons to Natural Stimuli. Science. 2000; 289:1569. [PubMed: 10968796]
59. Meeks JP, Arnson HA, Holy TE. Representation and transformation of sensory information in the mouse accessory olfactory system. Nat Neurosci. 2010; 13:723–730. [PubMed: 20453853]
60. Kim CK, et al. Simultaneous fast measurement of circuit dynamics at multiple sites across the mammalian brain. Nat Methods. 2016; 13:325–328. [PubMed: 26878381]
61. Lehtoranta M, et al. Division of the male rat rhabdosphincter into structurally and functionally differentiated parts. Anat Rec A Discov Mol Cell Evol Biol. 2006; 288A:536–542.
62. Thor KB, de Groat WC. Neural control of the female urethral and anal rhabdosphincters and pelvic floor muscles. AJP Regul Integr Comp Physiol. 2010; 299:R416–R438.
63. Nout YS, et al. Telemetric monitoring of corpus spongiosum penis pressure in conscious rats for assessment of micturition and sexual function following spinal cord contusion injury. J Neurotrauma. 2005; 22:429–441. [PubMed: 15853461]
64. Soukhova-O'Hare GK, Schmidt MH, Nozdrachev AD, Gozal D. A novel mouse model for assessment of male sexual function. Physiol Behav. 2007; 91:535–543. [PubMed: 17512960]

65. Bollig-Fischer A, Thakur A, Sun Y, Wu J, Liao DJ. The Predominant Proteins that React to the MC-20 Estrogen Receptor Alpha Antibody Differ in Molecular Weight between the Mammary Gland and Uterus in the Mouse and Rat. Int J Biomed Sci. 2012; 8:51–63. [PubMed: 23675257]

66. Saleh TM, Connell BJ, McQuaid T, Cribb AE. Estrogen-induced neurochemical and electrophysiological changes in the parabrachial nucleus of the male rat. Brain Res. 2003; 990:58–65. [PubMed: 14568330]

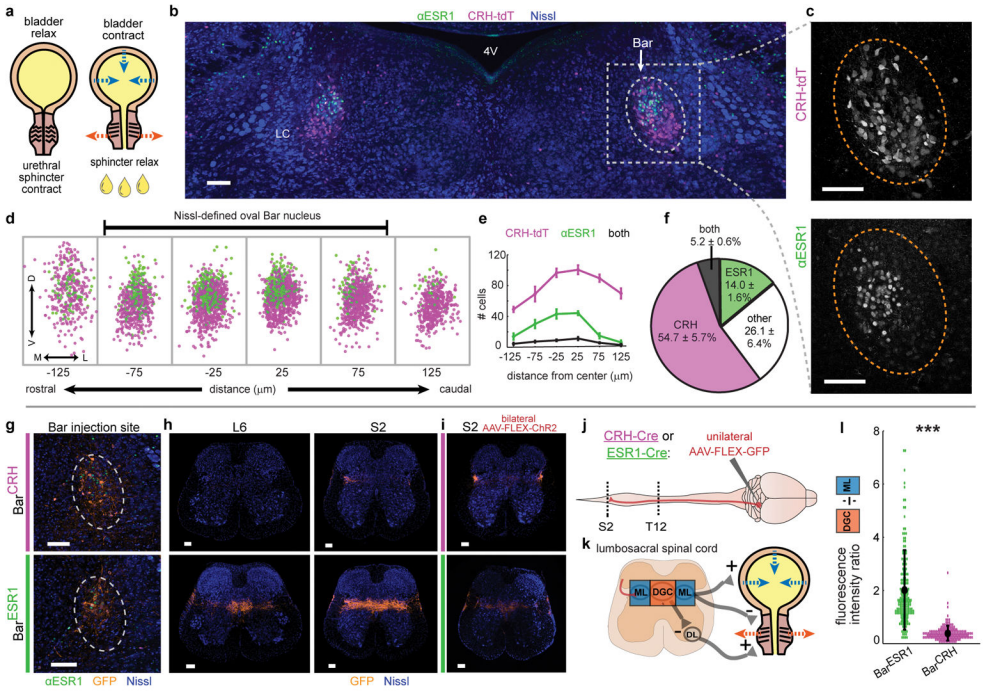

Fig. 1. A novel cell type in Barrington's nucleus with projections biased to sphincter-inhibiting interneurons

a, Urination requires sphincter relaxation. **b,** ESR1-immunostaining in Bar (dotted oval) in CRH-tdT mouse. LC = locus coeruleus, 4V = 4th ventricle. **c,** Larger view of CRH-tdT (top) and αESR1 (bottom) channels from (b)**. d,** Rostrocaudal overlay of αESR1 cells (green) in Bar registered to centroid of CRH-tdT cells (magenta). **e,** Cell counts, and **f**, cell percentages in Bar (mean ± s.e.m., n=6 mice). **g**, GFP expression at Bar injection site in CRH-Cre (top) or ESR1-Cre (bottom) individuals. **h**, Axonal projections in lumbosacral spinal cord (right L6, left S2) for injections in (g). **i**, Axonal projections in lumbosacral S2 spinal cord for injection sites in Fig. 3b. **j**, Schematic for identifying Bar cell type axonal projections to spinal cord. **k**, Simplified urinary circuitry in the lumbosacral spinal cord. ML = mediolateral column, DGC = dorsal grey commissure, DL = dorsolateral nucleus. **l**, Quantification of Bar^{ESR1} and Bar^{CRH} axonal projections in lumbosacral spinal cord. Points are individual sections, thick black line is mean ± s.e.m for Bar^{CRH} (magenta, n=10 mice), Bar^{ESR1} (green, n=10 mice). Scale bars = 100 μm. ***p=0.00018 (Mann-Whitney U test).

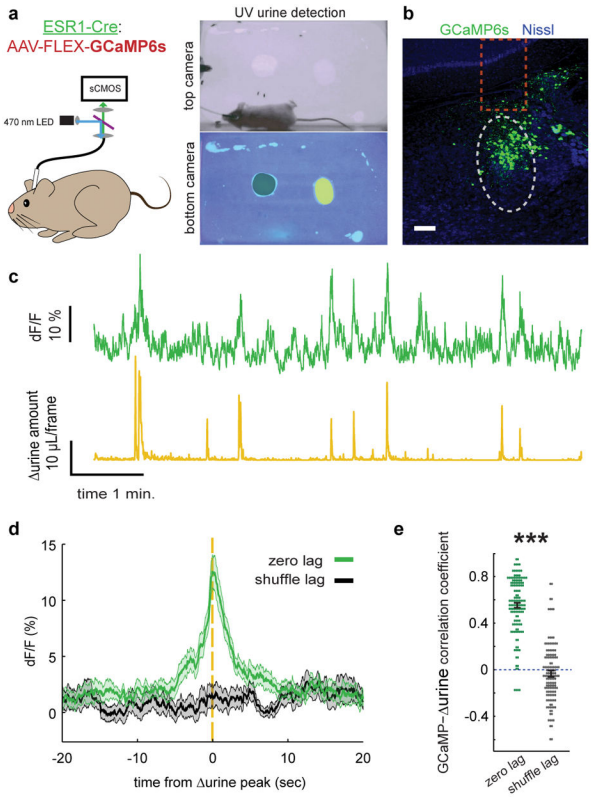

Fig. 2. Bar^{ESR1} activity increases during urination events

a, Schematic of fiber photometry experiment and example urine quantification with control odor (black shading) and female odor (yellow shading) on bottom camera view. **b**, Example GCaMP6s expression in Bar (grey dotted oval) of ESR1-Cre mouse. Dotted orange rectangle shows approximate fiber location. **c**, Example Bar$^{ESR1\text{-}GCaMP6s}$ fluorescence (top green) and derivative of urine detection (Δurine, bottom yellow). **c**, Example GCaMP6s expression in Bar (grey dotted oval) of ESR1-Cre mouse. Dotted orange rectangle shows approximate fiber location. **d**, GCaMP6s fluorescence synchronized to Δurine peaks (green) or at shuffled times (black) for all mice (thick line and shading are mean ± s.e.m., n=76 urination events from 7 mice). **e**, Correlation coefficient between GCaMP6s and Δurine traces at zero lag (green) and random lag (grey) for all mice (mean ± s.e.m., same events as panel n). Scale bar = 100 μm. ***p=1.1E-40 (Mann-Whitney U test).

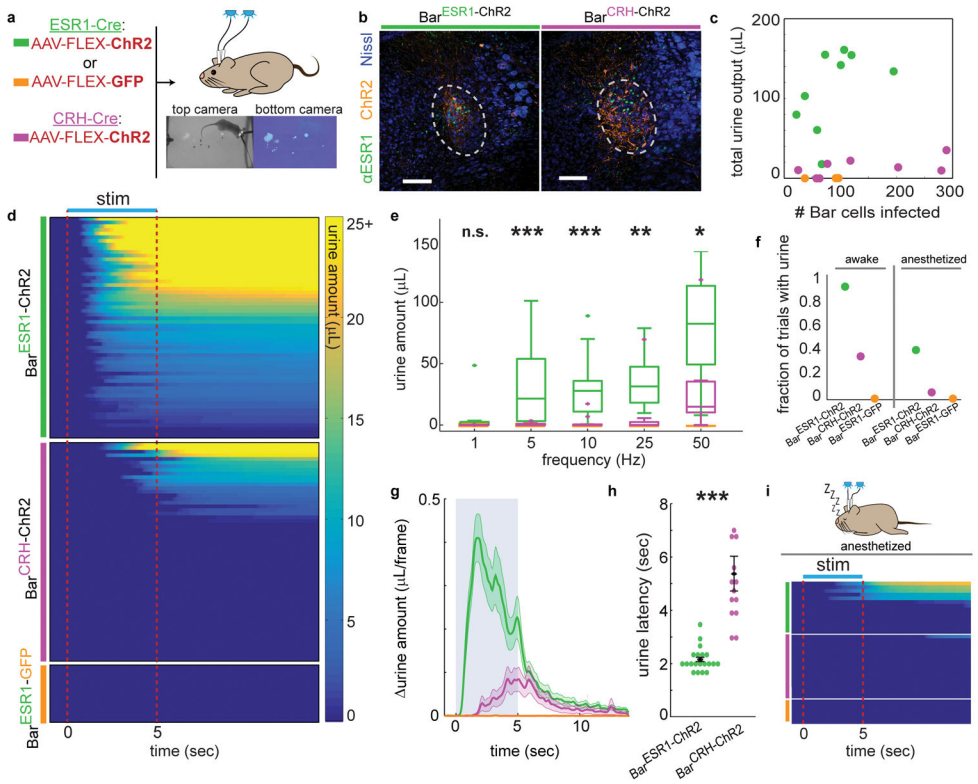

Fig. 3. Photostimulation of Bar^{ESR1} neurons induces efficient urination in awake and anesthetized animals

a, Schematic of optogenetic stimulation and example urine detection. **b,** Example ChR2 expression in ESR1-Cre (left) or CRH-Cre (right) individuals. **c,** Total urine output across all trials for each individual versus ChR2 expression. **d,** Heatmap of urine output following awake photostimulation for all trials >10Hz (n=10 Bar$^{ESR1\text{-}ChR2}$, 10 Bar$^{CRH\text{-}ChR2}$, 3 Bar$^{ESR1\text{-}GFP}$ mice), sorted by decreasing total urine amount. **e,** Urine amounts at different photostimulation frequencies: boxplots show median, 25th/75th quartiles, 1.5x interquartile ranges, and outlier dots outside these ranges (n=20 trials from 10 mice, p=0.42, 0.00049, 0.00096, 0.0021, 0.011 for 1, 5, 10, 25, 50 Hz, Mann-Whitney U test for Bar$^{ESR1\text{-}ChR2}$ compared to Bar$^{CRH\text{-}ChR2}$ at each frequency). Quartile range boxes are condensed at zero when most trials do not have any urine. **f,** Fraction of trials with photostimulated urine detected in panels (d), awake, and (i), anesthetized. **g,** Δurine amount around 50 Hz photostimulation (blue shading; same mice as panel d; thick line and shading are mean ± s.e.m, n=20 trials from 10 mice). **h,** Urination latency after 50 Hz photostimulation (same trials as panel g), mean ± s.e.m, p=1.7E-6, Mann-Whitney U test. **i,** Heatmap of urine output around anesthetized photostimulation for all trials (n=7 Bar$^{ESR1\text{-}ChR2}$, 8 Bar$^{CRH\text{-}ChR2}$, 3 Bar$^{ESR1\text{-}GFP}$ mice). Scale bars = 100 µm. Colors for all panels: green = Bar$^{ESR1\text{-}ChR2}$, magenta = Bar$^{CRH\text{-}ChR2}$, orange = Bar$^{ESR1\text{-}GFP}$.

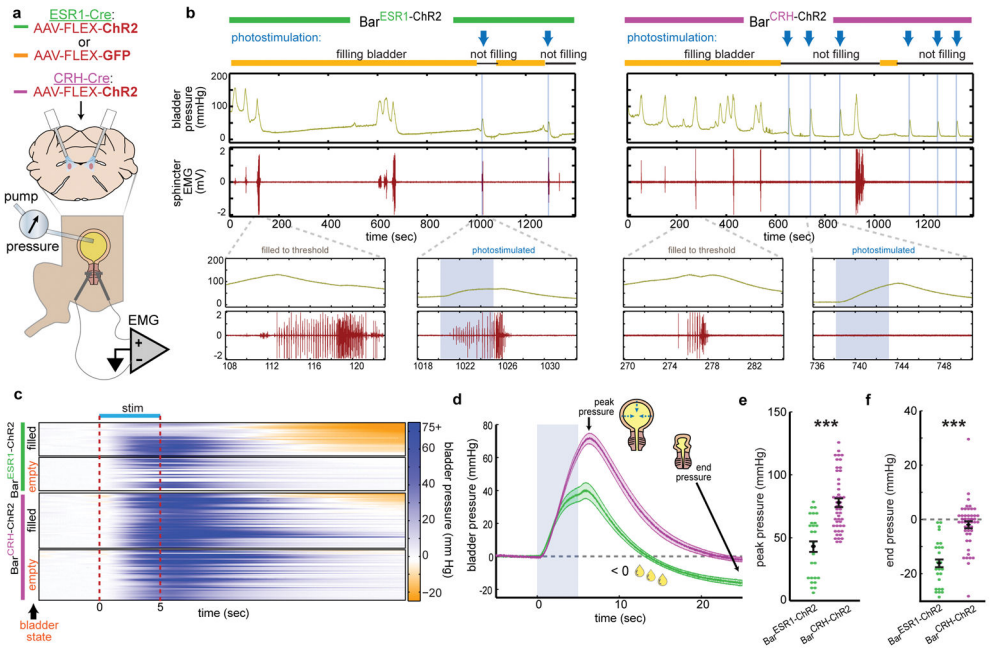

Fig. 4. Bar^{ESR1} neurons facilitate urine release during cystometry

a, Schematic for optogenetic Bar stimulation during cystometry. **b,** Representative raw bladder pressure and EUS EMG traces for Bar$^{ESR1\text{-}ChR2}$ (left) and Bar$^{CRH\text{-}ChR2}$ (right) individuals. Blue arrows and shading indicate photostimulation times, and yellow/black lines denote cystometry pump on/off. Top traces are 20 minutes; bottom traces show 15 second detail when the bladder is filled to threshold (no photostimulation) versus when Bar is photostimulated (blue shading). **c,** Heatmap of bladder pressure, sorted by increasing end pressure (decreasing urine release), around photostimulation for both filled and empty bladder trials (n=3 Bar$^{ESR1\text{-}ChR2}$, top, and 5 Bar$^{CRH\text{-}ChR2}$, bottom, mice). **d,** Bladder pressure for 'filled' bladder data in panel (c), showing peak and end pressure where negative pressure indicates urine release (thick line and shading are mean ± s.e.m., green = Bar$^{ESR1\text{-}ChR2}$, magenta = Bar$^{CRH\text{-}ChR2}$). **e,** Peak and **f,** end bladder pressure from (d), mean ± s.e.m,p=6.8E-6 and p=4.7E-8, respectively (Mann-Whitney U test).

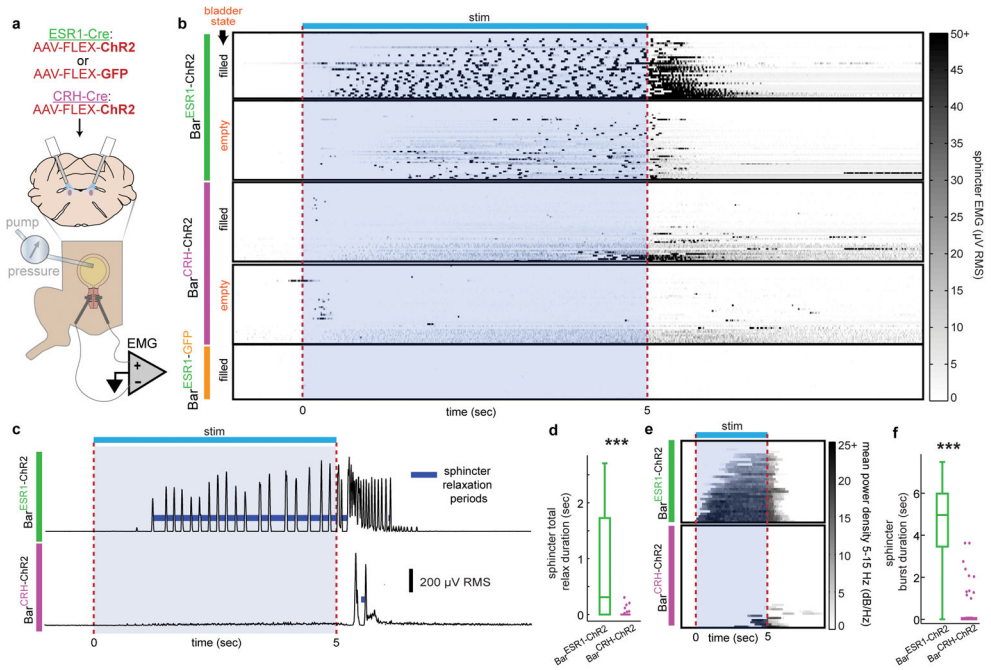

Fig. 5. Bar^{ESR1} neurons relax the urethral sphincter by promoting bursting activity

a, Schematic for optogenetic Bar stimulation during cystometry and urethral EMG recording. **b,** Heatmap of EUS EMG, sorted by increasing mean voltage, around photostimulation for both filled and empty bladder trials (n=6 Bar$^{ESR1\text{-}ChR2}$, top, 5 Bar$^{CRH\text{-}ChR2}$, middle, and 3 Bar$^{ESR1\text{-}GFP}$, bottom, mice). **c**, Example RMS EMG traces from single 'filled' bladder trials in (b), showing calculated sphincter relaxation periods (dark blue) between bursts. **d,** Total sphincter relaxation time boxplot (median, 25th/75th quartiles, 1.5x interquartile ranges, and outlier dots outside these ranges) for 'filled' bladder trials in (b), n=33 Bar$^{ESR1\text{-}ChR2}$ trials and n=48 Bar$^{CRH\text{-}ChR2}$ trials, ***p=2.4E-8 (Mann-Whitney U test). **e,** Heatmap of mean EMG power density at bursting frequencies (5–15 Hz) for 'filled' bladder trials in (b) (Bar$^{ESR1\text{-}ChR2}$, top, and Bar$^{CRH\text{-}ChR2}$, bottom). **f,** Sphincter burst duration boxplot for trials in (e), n=33 Bar$^{ESR1\text{-}ChR2}$ trials and n=48 Bar$^{CRH\text{-}ChR2}$ trials, ***p=1.1E-11 (Mann-Whitney U test). Quartile range boxes in (d) and (f) are condensed at zero when most trials do not have any bursting.

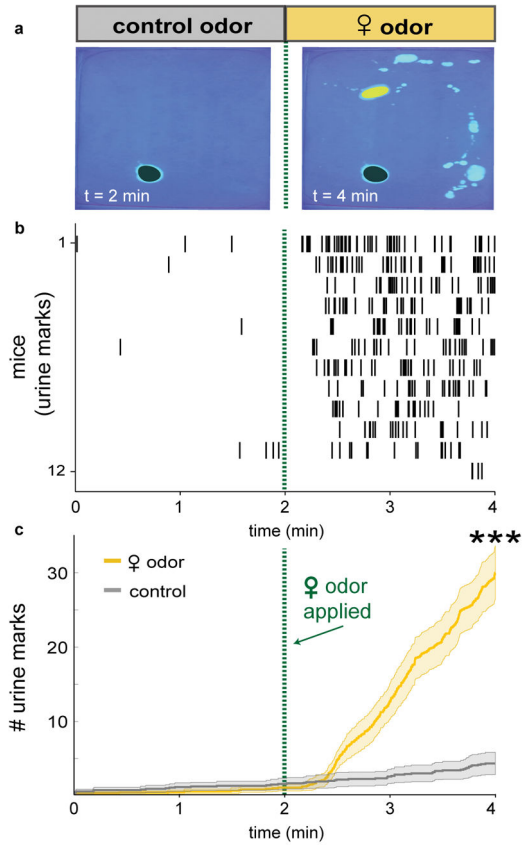

Fig. 6. Naïve male mice rapidly and robustly scent mark to female odor cues

a, Scent marking behavior in wild-type mice. Left: after 2 min. exposure to control odor (black shading), right: after additional 2 min. with female odor (yellow shading). **b,** Raster plot of urine marks detected. **c,** Urine marks during habituation with control odor only (grey) or with female odor (yellow) (thick line and shading are mean ± s.e.m., n=12 mice). ***p=0.00049 (Wilcoxon signed rank) for number of urine marks at 2 min. and 4 min.

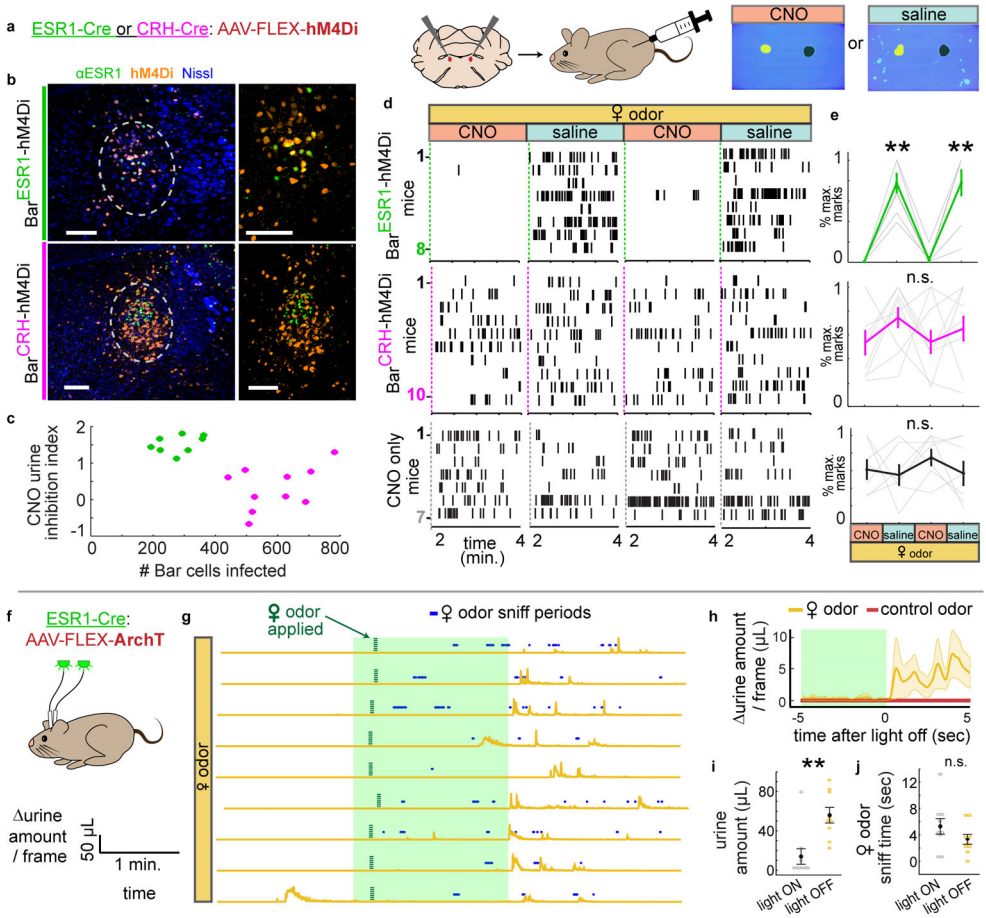

Fig. 7. Chemogenetic and optogenetic inhibition of Bar^{ESR1} neurons impairs voluntary scent marking urination

a, Schematic of chemogenetic inhibition of Bar during scent marking urination. **b,** Example hM4Di expression in Bar of ESR1-Cre, top, and CRH-Cre, bottom, mice; larger views minus Nissl on the right**. c,** Number of Bar cells infected with hM4Di virus versus CNO urine inhibition index (see Methods) for all mice (green for ESR1-Cre, magenta for CRH-Cre). **d,** Raster plots of urine marks on consecutive days with either CNO or saline (Bar$^{ESR1\text{-}hM4Di}$, top, Bar$^{CRH\text{-}hM4Di}$, middle, CNO-only control, bottom). **e,** Percentage of maximum urine marks across all CNO or saline days for, top, Bar$^{ESR1\text{-}hM4Di}$ (n=8, p=0.00013 Friedman's test, **day 2 saline p=0.0058, day 4 saline p=0.011 Dunn-Sidak posthoc differences from CNO days 1 & 3, middle, Bar$^{CRH\text{-}hM4Di}$ (n=10, p=0.29 Friedman's test) and, bottom, CNO control (n=7, p=0.86 Friedman's test) mice (thin lines individual mice, thick lines mean ± s.e.m.). **f,** Schematic of optogenetic inhibition of Bar^{ESR1} during scent marking urination. **g,** Δurine amount around 2 min. photoinhibition period. Female odor presented within 15 seconds of light on, and subsequent sniff periods shown in blue. n=9 trials from 3 mice. **h,** Δurine amount ± 5 sec. from end of photoinhibition for control odor and female odor (thick line and shading are mean ± s.e.m., n=9 total trials from 3 mice). **i,** Urine amount (**p=0.0039), and, **j**, female odor sniff time (p=0.20) during 2 min. photoinhibition period and 2 min. immediately following (mean ± s.e.m., same trials as h,

Wilcoxon signed rank tests). Green shading denotes photoinhibition periods. Scale bars = 100 μm.